Equatorial Solitary Waves. Part V: Initial Value Experiments, Coexisting Branches, and Tilted-Pair Instability

JOHN P. BOYD

Department of Atmospheric, Oceanic and Space Science, University of Michigan, Ann Arbor, Michigan

(Manuscript received 27 June 2001, in final form 12 February 2002)

ABSTRACT

A series of high-resolution numerical experiments, augmented by theory, to further explore the dynamics of equatorial dipole vortices (Rossby solitary waves) is performed. When the amplitude is sufficiently large so that the vortices trap fluid internally, the solitary waves for a given phase speed are not unique. The potential vorticity–streak function (q–Ψ) relationship is everywhere linear for one branch, but highly nonlinear in the recirculation region for the second branch. Westward-traveling vortex pairs are highly unstable on the midlatitude beta plane, but the equatorial wave guide stabilizes vortex pairs that straddle the equator, even when given a strong initial tilt. As discovered by Williams and Wilson and explained theoretically by Boyd, the author confirms that higher latitudinal mode solitary waves are weakly nonlocal through radiation of sinusoidal Rossby waves of lower latitudinal mode number. The amplitude and wavelength of the radiation are in good agreement with nonlocal soliton theory.

It is sometimes said that the great discovery of the nineteenth century was that the equations of nature were linear, and the great discovery of the twentieth century is that they are not.—Thomas Körner, *Fourier Analysis* (1988, p. 99)

1. Introduction

Equatorially trapped waves are a dominant feature of both the tropical ocean and atmosphere. Since the Navier–Stokes equations are nonlinear, it would seem obvious to explore the nonlinear dynamics of these waves. However, a quarter century of study of nonlinear equatorial waves can be summarized on a single page (Table 1).

Equatorial Rossby solitary waves are easily generated by very unsolitonic forcing or initial conditions (Kindle 1983; Greatbatch 1985; Williams and Wilson 1988): the flow spontaneously evolves to a state with one or more solitary waves propagating at a steady faster-than-linear speed to the west. Latitudinal shear (Greatbatch 1985; M.-T. Li 1983, personal communication; Li 1984) and east–west variations in thermocline depth (Marshall and Boyd 1987; Long and Chang 1990) do not inhibit soliton formation or qualitatively modify the theory, at least if weak.

Showman and Dowling (2000) have numerically modeled equatorial plumes on Jupiter, which are long-lived bright cloud streaks as much as 10 000 km wide. Infinitesimal amplitude Rossby waves of the proper scale disperse rapidly, but nonlinear Rossby waves have the observed longevity and coherence. (Unlike the disturbances studied below, equatorial plumes seem to lack recirculating fluid, and thus are of only moderate amplitude). Thus, a solitary wavelike coherence has been observed in equatorial Rossby waves on other worlds.

Nevertheless, Rossby solitary waves have not been identified in the tropical ocean, either observationally or in general circulation models. Existing theory implies that solitons should be as common as cockroaches. [Indeed, the equatorial Rossby soliton has become a popular test problem for oceanic numerical models (Haidvogel and Beckmann 1999, 204–209).] Our goal is to extend the theoretical frontier in hopes of eventually resolving this mystery, either by finding an X factor that suppresses solitary waves or forging a club to thrash observationalists and modelers into looking for solitons.

For numerical and analytical simplicity, we shall restrict our pursuit of extensions to the 1½-layer model: a dynamically active upper layer that models the flow above the thermocline and an infinitely deep, motionless, lower layer. The equations of motion for the upper layer are then identical to the usual shallow-water wave equations if the upper-layer depth is multiplied by the fractional density difference between the two layers to obtain the so-called ''equivalent depth.'' In the tropical ocean, the upper layer is on the order of a hundred meters and the equivalent depth is about a half meter.

Corresponding author address: Dr. John P. Boyd, Department of Atmospheric, Oceanic and Space Science, University of Michigan, 2455 Hayward Avenue, Ann Arbor, MI 48109.
E-mail: jpboyd@ergineumich.edu

TABLE 1. Selected bibliography of nonlinear equatorial waves.

Reference	Comments
Domaracki and Loesch (1997)	Resonant triad interaction
Loesch and Deininger (1979)	
Boyd (1980b)	Kelvin frontogenesis through strained coordinates
Boyd (1980a)	KdV theory of Rossby solitons
Jain et al. (1981)	Envelope (NLS-type) solitary waves and nonlinear wavepackets
Ripa (1982)	Kelvin frontogenesis via simultaneous triad resonance
Ripa (1983a,b)	Comprehensive study of resonant triads
Boyd (1983a)	Nonlinear wavepackets and solitons solving NLS equation
Boyd (1983b)	Longwave/shortwave resonance
Boyd (1983c)	Second harmonic resonance
Kindle (1983)	Generation of robust, multiple Rossby solitons by impulsive wind jumps
M.-T. Li (1983*, 1984)	Rossby solitons in weak shear
Boyd (1984)	Kelvin KdV solitons in a shear flow
Ripa (1985)	Improved theory of nonlinear Kelvin waves
Greatbatch (1985)	Numerical: Rossby solitons in El Niño; Analytical: Rossby solitons in weak latitudinal shear
Boyd (1985)	Rossby modons (large amplitude dipoles)
Wu (1986)	Heuristic derivation of KdV Rossby solitons
Marshall and Boyd (1987)	Theory of KdV and NLS solitons in continuous stratification
Williams and Wilson (1988)	Rossby soliton–soliton collisions Radiative decay of large amplitude higher *y*-mode solitons
Boyd (1989b)	Weakly nonlocal Rossby solitary waves
Long and Chang (1990)	Kelvin frontogenesis or soliton-formation in zonally varying thermocline
Boyd (1991a)	Review
Ma (1992)	Reflection of Rossby solitons from western coast
Ma (1996)	North Brazil retroflection eddies as coherent equatorial structures
Williams (1996)	Numerical illustration of slow barotropic decay of baroclinic Rossby soliton
Boyd (1998b)	Monograph on nonlocal solitons (including equatorial)
Boyd (1998a)	Improved theory including gravity wave resonance for Kelvin frontogenesis (front curvature)
Zheng et al. (1998)	Observations of Kelvin solitary waves
Matsuura and Iizuka (2000)	Kelvin breaking in El Niño
Milewski and Tabak (1999)	Finite-depth effects of nonlinear equatorial waves
Fedorov and Melville (2000)	Resonance theory of Kelvin frontogenesis; steadily translating fronts smoothed by horizontal viscosity
Showman and Dowling (2000)	Equatorial plumes on Jupiter, long-lived only because of nonlinearity
Boyd (2002)	Numerical methods for nonlocal equatorial waves
Boyd (2002)**	Weakly nonlocal Kelvin fronts and solitons

* Personal communication.
** Manuscript submitted to *J. Phys. Oceanogr.*

The time-dependent shallow-water wave equations are

$$u_t + uu_x + vu_y - yv + h_x = 0 \quad (1)$$

$$v_t + uv_x + vv_y + yu + h_y = 0 \quad (2)$$

$$h_t + \{uh\}_x + \{vh\}_y = 0, \quad (3)$$

where u and v are the east–west and north–south velocities, and h is the total depth of the fluid. Later graphs will sometimes display deviation from the unit mean depth,

$$\phi(x, y, t) \equiv h(x, y, t) - 1. \quad (4)$$

The equations have been nondimensionalized in the way standard in equatorial dynamics (Moore and Philander 1977). A unit length scale is about 300 km, or 3° of longitude, and the velocity scale is about 2 m s^{-1}.

In the next section, we review a couple of theorems on the mass streakfunction and Bernoulli function. (The ''streakfunction'' is the streamfunction in a frame of reference traveling with the solitary wave.)

When the vortex is free of recirculating fluid, or outside of the region of trapped fluid when there is one, we prove that the potential vorticity must be a *linear* function of the streakfunction Ψ whereas the Bernoulli function must be *quadratic* in Ψ.

Section 3 describes new features of the numerical model, otherwise identical with Boyd (1998a), which are necessary to compute and analyze solitary waves.

The next two sections describe experiments on large amplitude solitary waves. Within the region of closed streaklines, the q–Ψ and B–Ψ relations are nonlinear and nonparabolic, respectively, for one class of dipolar vortex solitons. However, for a given phase speed, there is a second class of solutions for which these relationships are linear (q–Ψ) and parabolic (B–Ψ) *everywhere* both inside and outside the recirculation region.

Midlatitude vortex dipoles, if traveling westward, are *unstable* to spontaneous rotation of the line connecting the two vortex centers. Our numerical experiments (sec. 6) with ''tilted dipole'' initial conditions show that the equatorial waveguide *suppresses* this instability. Westward-traveling equatorial modons seem to be highly stable.

Williams and Wilson (1988) observed that as the amplitude increased, higher latitudinal mode (quadrapole vortex) solitons radiated energy in the form of $n = 1$ Rossby waves. Boyd (1989a,b) explained their observations through the theory of nonlocal solitary waves. In section 7, we illustrate this theory through very high resolution numerical solutions combined with Fourier transform analysis of the emitted radiation.

The final section is a discussion of unresolved issues.

2. Theorems: Mass streakfunction and modified Bernoulli function

The velocities in the shallow-water equations can be expressed in terms of h plus a single scalar function ψ via

$$uh = -\psi_y - \left\{\int^x h_t(x', y)\, dx'\right\}_t; \qquad vh = \psi_x, \quad (5)$$

where ψ will be dubbed the ''mass-weighted streamfunction.'' (Proof: direct substitution into the equation of continuity.)

In a frame of reference traveling at a phase speed c, the shallow-water equations become

$$u_t + (u - c)u_x + vu_y - yv + h_x = 0 \quad (6)$$

$$v_t + (u - c)v_x + vv_y + yu + h_y = 0 \quad (7)$$

$$h_t - ch_x + \{uh\}_x + \{vh\}_y = 0, \quad (8)$$

where in a minor abuse of notation, the same symbol ''x'' is used for nondimensional longitude in both the earth-fixed and moving coordinate systems. (The explicit appearance of c in the equations of motion always indicates that they are written in a moving reference frame.) The corresponding streamfunction in the moving reference frame is usually called the ''streakfunction'' Ψ and is related to the streamfunction via

$$\Psi = \psi + cy. \quad (9)$$

If the solution is a wave that is steadily translating at the same speed c as used to define the moving reference frame, then the solution is *independent of time* in the moving reference frame. The mass-weighted velocities are then

$$(u - c)h = -\Psi_y; \qquad vh = \Psi_x, \quad (10)$$

where $(u - c)$ is the east–west velocity as observed in the moving reference frame. The equation of continuity is trivially satisfied; the two momentum equations become a system of two equations for the two unknowns (h, Ψ).

We can prove the following theorems.

Theorem 1 (Potential vorticity)

1) The potential vorticity

$$q \equiv \frac{v_x - u_y + y}{h} \quad (11)$$

is *exactly* conserved for the equatorial, nonlinear inviscid shallow-water wave equations.

2) For a *steadily translating* disturbance moving east–west at a constant phase speed c, q conservation is equivalent to

   a) The Jacobian of q and Ψ is *zero*:

$$J(q, \Psi) = 0 \Leftrightarrow -\Psi_y q_x + \Psi_x q_y = 0, \quad (12)$$

   b) The potential vorticity is a *function of the streakfunction only*, that is, for some function F

$$q = F(\Psi), \quad (13)$$

3) If the disturbance is a *localized disturbance* that tends to *zero at infinity*, then on *open streaklines*, that is, isolines of Ψ that extend to *spatial infinity* where $u, v, \phi \to 0$,

$$q = \frac{\Psi}{c} \equiv F(\Psi) \quad \text{(open streaklines only)}. \quad (14)$$

Proof: Conservation of potential vorticity is shown by Ripa (1982). Proposition 2a is proved by writing $Dq/dt = 0$ in the moving coordinate system, then dropping the time-derivative (because a steadily moving disturbance does not depend on time in the moving reference frame) and replacing the velocities by derivatives of the mass streakfunction. Proposition 2a is equivalent to $\Psi_y/\Psi_x = q_y/q_x$, which asserts that the isolines of Ψ and q are everywhere parallel. This is possible if and only if $q = F(\Psi)$ for some function F so that the value of the potential vorticity is the same everywhere along a given isoline of Ψ, and vice versa. Proposition 3 is proved by noting that for an isolated disturbance, $\psi \to 0$ as $(x^2 + y^2) \to \infty$. This implies that $h \to 1$, $q \to y$, $\Psi \to cy$. The only function $F(\Psi)$ that is compatible with these limits is $F(\Psi) = \Psi/c$. The arguments for Propositions 2 and 3 are identical to those of modon theory.

The quantity B defined below is a close cousin of the usual Bernoulli function $h + (1/2)u^2 + (1/2)v^2$.

Theorem 2 (Modified Bernoulli Function)

1) The *modified* Bernoulli function

$$B \equiv \frac{1}{2}cy^2 + \phi + \frac{1}{2}([u - c]^2 - c^2 + v^2) \quad (15)$$

is *exactly* conserved following the motion for a *steadily translating* disturbance moving east–west at a *constant* phase speed c. *B conservation* is equivalent to

   a) The Jacobian of B and Ψ is zero:

$$J(B, \Psi) = 0 \Leftrightarrow -\Psi_y B_x + \Psi_x B_y = 0, \quad (16)$$

b) The *modified* Bernoulli function is a function of the *streakfunction only*; that is,

$$B = G(\Psi) \tag{17}$$

for some function G. [Moore and Niler (1974) note that $G(\Psi) = dF/d\Psi$, where $F(\Psi)$ is the streakfunction–vorticity functional of the previous theorem]

2) If the disturbance is a *localized disturbance* that tends to *zero* at *infinity*, then on *open streaklines*; that is, isolines of Ψ that extend to *spatial infinity* where $u, v, \phi \to 0$:

$$B = \frac{1}{2c}\Psi^2 \equiv G(\Psi) \quad \text{(open streaklines only)}. \tag{18}$$

Proof: To demonstrate Proposition 1, note that B is conserved following the motion if and only if the quantity $R \equiv (u - c)B_x + vB_y$ is zero. However, it is easy to verify by explicit differentiation and substitution from the momentum equations that $-qhv + B_x = 0$ and $qh(u - c) + B_y = 0$. (Indeed, these equations are variants of the usual longitudinal and latitudinal momentum equations.) Substitution for B_x and B_y in R demonstrates that $R \equiv 0$. Propositions 2 and 3 then follow by recycling the arguments used to prove similar propositions in the preceding theorem.

3. Numerical model

a. Overview

The model is the same as Boyd (1998a) except for the addition of a few new features. The novelties are described in succeeding subsections; older features are reviewed only briefly in the rest of this subsection.

The model employs third-order Adams–Bashforth explicit time marching together with centered eighth-order time differencing. (Fourth-order Runge–Kutta was used for the first two time steps.) The boundary conditions are periodicity in x with period P and decay to zero for large y, which was approximated by a finite limit $y_{\max}$. Most experiments assumed equatorial symmetry, but an unsymmetric version was also run to examine the stability of initially tilted dipolar vortices.

The model usually employed a moving frame of reference where the constant translational velocity of the coordinate system, c_{trans}, was chosen to roughly mimic the expected phase speed c of the coherent structures so as to keep them approximately centered. [The equations in the moving frame are simply (6)–(8) above)].

b. Boundary damping (''sponge layer'')

Heavy damping near the boundaries at $x = \pm P/2$, a device often called a ''sponge layer,'' was applied to eliminate gravity wave and Kelvin wave transients and prevent them from reentering the domain through the spatial periodicity and thus contaminating the solitary waves. The boundary damping was a linear friction, equivalent to modifying the zonal momentum equation to

$$u_t = -\gamma(x)u + \{\ \}, \tag{19}$$

where the empty braces represent the other terms in the x-momentum equation, and similarly for the latitudinal momentum and continuity equations. Because the sponge layer is a computational artifice, it is pointless to implement it in a time-accurate fashion. Instead, every n_b time steps, the east–west velocity at the end of a time step of length τ was updated as

$$u^{\text{damped}} = u - n_b\tau\gamma(x), \tag{20}$$

which was then used to reinitialize the calculation and similarly for the other components. This is equivalent to a first-order, forward Euler time-marching implementation of the friction.

The friction was somewhat arbitrarily chosen as

$$\gamma(x) = \gamma_b\{\exp(-\Xi[x - P/2]^2) + \exp(-\Xi[x + P/2]^2)\}, \tag{21}$$

where γ_b and Ξ are constants, typically 1/20 and 1/4. (Note that the sponge layers move with the reference frame and thus are fixed at the ends in the moving frame.) The Gaussian form ensures that the damping is smooth but extremely small at the center of the interval. The peril is that, if Ξ is too small, the damping will vary so rapidly that it will reflect a large amount of waves back into the center of the domain—precisely what we wish to avoid. However, a WKB method of multiple scales argument shows that such reflection is very small for all waves of east–west wavenumber k such that $k \gg \Xi$.

c. Hyperviscosity

A hyperviscosity proportional to the cube of the Laplace operator was applied every few time steps to dissipate very small scale features. The coherent structures are not sensitive to the hyperviscosity so long as it is sufficiently weak, with the by no means trivial exception that the model blew up if the damping were completely omitted!

As for the boundary friction, the hyperviscosity

$$u_t = \nu\nabla^3 u \tag{22}$$

was implemented by applying the filter step

$$u^{\text{damped}} = u + n_h\tau\nu\nabla^3 u \tag{23}$$

every n_h time steps where τ is the time step. Typically, $n_h = 20$.

The shortest wave on a grid of length h has a wavelength of $2h$ and a wavenumber of π/h. The longest wave, excluding the zonal mean, that fits on a box of period P has wavenumber $(2\pi/P)$. The e-folding scales D of these extreme components are

$$D_{2h} = \nu\frac{\pi^6}{h^6}, \qquad D_{\text{longest}} = 32\nu\frac{\pi^6}{P^6}, \tag{24}$$

where the *e*-folding scale is defined as usual as the time required for a given wave to decay in amplitude by a factor of $\exp(-1)$. In most experiments, D_{longest} was $O(10^9)$ or larger while D_{2h} was $O(1)$ in nondimensional time units.

Hyperviscosity allows potential vorticity contours to break and reconnect. Such topological changes in the isolines of potential vorticity are impossible for an *inviscid* fluid, where the contours may stretch and stretch but can never break or merge. However, the isolines merge at very fine scales; the larger patterns, such as the merger of two nearly circular vortices into one, are independent of the details of a scale-selective dissipation as long as it is weak and nonzero.

d. Phase speed computation

If the boundary damping and hyperviscosity do their job, the flow will evolve to a single coherent structure in the center of the domain. However, the translational speed of the moving frame of reference, c_{trans}, is never exactly equal to the phase speed c of the coherent structure. The speed can be corrected by noting that, if the disturbance is a steadily translating coherent structure, the time-dependence can be reduced to zero by adjusting the speed of the frame of reference. Let δc denote the correction to the translational speed c_{trans}. Altering the phase speed is equivalent to adding $-\delta c u_x$ to the zonal momentum equation, $-\delta c v_x$ to the north–south momentum equation, and $-\delta c \phi_x$ to the continuity equation. The goal is to choose δc so as to minimize the integral of the time dependence over all space (excluding the sponge layers). Denoting the area integral by $\langle , \rangle$, which was approximated simply by an unweighted sum over all grid points, one finds

$$c \approx c_{\text{trans}} - \frac{\langle u_x, u_t\rangle + \langle v_x, v_t\rangle + \langle \phi_x, \phi_t\rangle}{\langle u_x, u_x\rangle + \langle v_x, v_x\rangle + \langle \phi_x, \phi_x\rangle}. \tag{25}$$

Figure 1 shows how the phase speed varies for a typical case. When the initial condition is flinging gravity and Kelvin waves both east and west and there is strong nonlinear shape-shifting at the core of the coherent structure, the computed phase speed is meaningless. When the transients have been absorbed and the core of the soliton has altered to its final state, the computed phase speed asymptotes to a constant: the speed of the solitary wave.

e. Computation of the streakfunction

The streakfunction can be computed by either integrating $\Psi_x = v$ and using the relationship $\Psi \sim cy$ far from the coherent structure to initialize the integration, or by integrating in y. Both approaches require a good estimate for the phase speed c. We chose to integrate

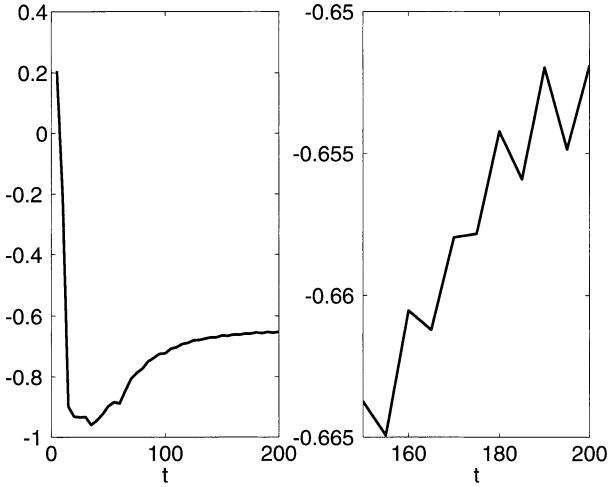

FIG. 1. Computed phase speed for a case initialized with the first-order KdV perturbation theory for $\epsilon = 0.9$, which corresponds to a minimum nondimensional east–west velocity of -1.02, a very large amplitude initial condition. After a tumultous adjustment phase with much radiation from the initial peaks, a steadily translating solitary wave evolves and the computed c converges to the soliton's phase speed. Left: c vs t; right: c vs t at late times.

$\Psi_y = u - c$ where u is the zonal velocity in the earth-fixed coordinate system. Since all the coherent structures turned out to be symmetric with respect to the equator, implying that the streakfunction is antisymmetric (with the proper choice of the arbitrary additive constant), we can impose the boundary condition $\Psi(x, y = 0) = 0$. The integration formula was

$$\Psi(y + h) = \Psi(y) + \frac{h}{3.6288 \times 10^6} \times \sum_{j=-4}^{4} I_j(u(y + jh) - c)\{1 + \phi(y + jh)\}, \tag{26}$$

where h is the latitudinal grid spacing and

$$\begin{aligned} I_{-4} &= 2497 & I_{-3} &= -25\,706 & I_{-2} &= 126\,286 \\ I_{-1} &= -425\,762 & I_0 &= 2\,224\,480 & I_1 &= 1\,909\,859 \\ I_2 &= -216\,014 & I_3 &= 36\,394 & I_4 &= -3233, \end{aligned} \tag{27}$$

where the symmetry conditions $u(x, -y) = u(x, y)$ and $\phi(x, -y) = \phi(x, y)$ are used to supply values south of the equator whenever symmetry with respect to the equator is assumed.

The nonlinear eigenvalue solver used a different grid with latitudinal points at $y = h/2, 3h/2, 5h/2, \cdots$. Setting $y = -h/2$ in (26) and invoking the antisymmetry constraint $\Psi(-h/2) = -\Psi(h/2)$ shows

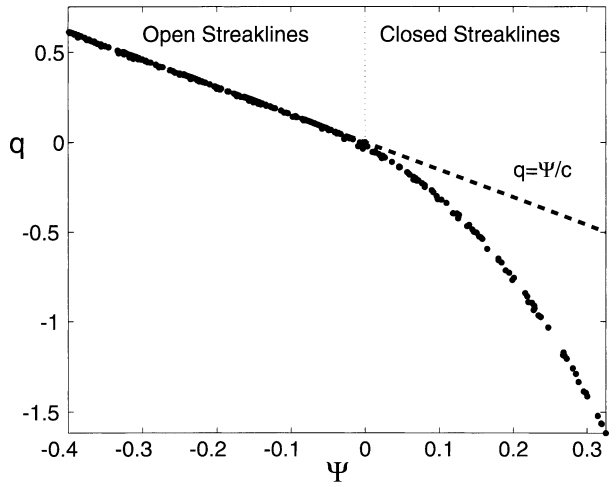

FIG. 2. Scatterplot of q–Ψ for perturbative initialization with $\epsilon = 0.9$. The potential vorticity $q(x, y)$ and streakfunction $\Psi(x, y)$ were evaluated at many points on a two-dimensional grid, and for each (x, y), the corresponding pair (q, Ψ) was plotted. According to theory, q and Ψ should be connected by a single function, $q = F(\Psi)$ for some function F. The dashed line is the linear function, $q = \Psi/c$, which must apply on open streaklines (left side) and does. However, theory says nothing about what happens on closed streaklines, and indeed the relationship between q and Ψ is highly nonlinear in the region of fluid which is trapped within the solitary wave, and moves with it (right of the dotted line).

$$\Psi\left(\frac{h}{2}\right) = \frac{1}{2}\frac{h}{3\,628\,800} \times \sum_{j=-4}^{4} I_j\left(u\left(-\frac{h}{2}+jh\right)-c\right)\left\{1+\phi\left(-\frac{h}{2}+jh\right)\right\}. \tag{28}$$

With this point known, Eq. (26) can be applied as before to compute Ψ at other latitudes.

4. Numerical experiments: $q - \Psi$ and $B - \Psi$ functions

In the KdV first-order perturbation theory of Boyd (1980a, 1985) for the $n = 1$ solitary wave, all streaklines are open for $\epsilon \leq 0.532$ but contain a region of recirculation for larger amplitude. (Here, ϵ is the ''pseudo-wavenumber'' such that the east–west velocity is proportional to $\text{sech}^2[\epsilon(x - ct)]$; the amplitude is proportional to ϵ^2.) When the perturbative solution was used as the initialization for ϵ smaller than the recirculation value, $\epsilon_{\text{recirc}} \approx 0.53$, the coherent structures that emerged did indeed have the linear q–Ψ relationship and quadratic B–Ψ functions predicted by the theorems above.

What happens for larger amplitude when recirculation occurs within a region of closed streaklines? Some analyses of midlatitude vortices have assumed that the open

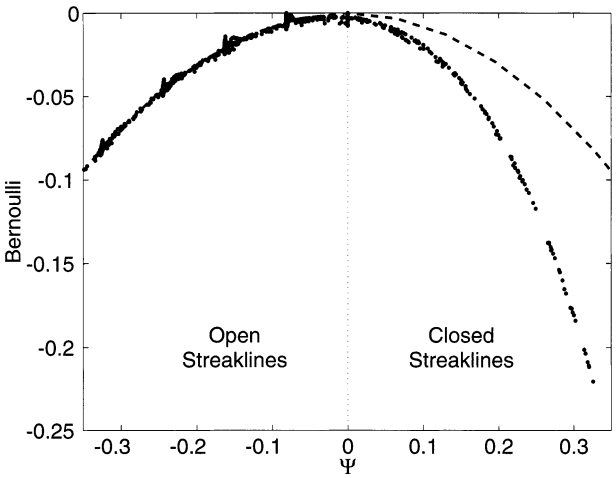

FIG. 3. Scatterplot of B–Ψ, same case as in Fig. 2.

streakline formulas apply on closed streaklines, too, so that $F(\Psi)$ and $G(\Psi)$ are analytic functions everywhere. Others have assumed that, as in modon theory, the potential vorticity/streakfunction relationship is linear but with a different slope in the recirculation region so that $F(\Psi)$ has a discontinuous slope at the outermost closed streakline. Still other studies have invoked the Prandtl–Batchelor Theorem (Batchelor 1956; Yamagata 1981; Matsuura and Yamagata 1985) to predict that potential vorticity is homogenized in the recirculation region so that $q = F(\Psi) =$ constant on all closed streaklines. This controversy about the likely form of $F(\Psi)$ is briefly reviewed in Mallier (1994, 1995), especially the earlier article.

The next two figures (Figs. 2, 3) show the results from an experiment that was initialized with the perturbative first-order approximation[1] for $\epsilon = 0.9$; the result was a solitary wave whose phase speed is $c \approx -0.65$. This experiment used a 320×40 grid on the spatial domain $x \in [-20, 20]$, $y \in [0, 5]$ (with equatorial symmetry assumed). It was integrated on $t \in [0, 200]$ with a time step of 1/200 and required about 1.5 hours of time on an Apple PowerMac G4 at 450 Mhz, averaging about 27 megaflops, not including graphics.

The figures clearly show that the $n = 1$ equatorial solitary wave conforms to none of the previously seen patterns. The potential vorticity and Bernoulli function do deviate markedly from the exterior forms on closed streaklines; in particular, $q(\Psi)$ becomes parabolic instead of linear. However, there is no obvious break in functional form or visible discontinuity of slope.

At spatial infinity, the function $q = F(\Psi)$ is *exactly* linear on open streaklines (Theorem 1, Proposition 3), and not merely approximately linear. The deviation from linearity on closed streaklines implies that $F(\Psi)$ cannot

[1] Due to a typo, the coefficient of ψ_2 for u was 10 times smaller than in the theory of Boyd (1985), but we did not rerun this case because the modified initialization is still legitimate.

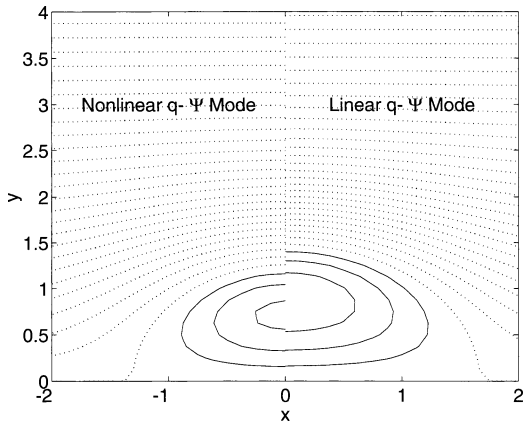

FIG. 4. Comparison of the two distinct, coexisting modes for $c = -0.645$. (Both modes are symmetric with respect to the midpoint of the graph, $x = 0$, and therefore both modes can be fully illustrated and compared by showing only one-half of each mode.) The contour interval was 0.1 for both halves of the diagram. The mode with the linear q–Ψ relationship was computed by solving a nonlinear eigenproblem (and then checked by substitution into our initial value code); the nonlinear mode was computed by time-dependent evolution in an initial value program.

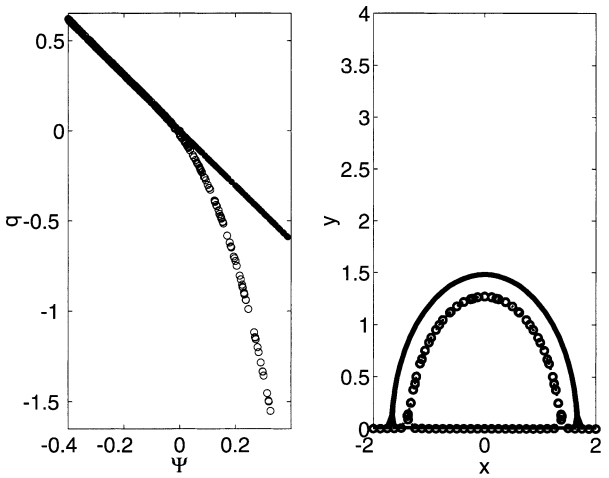

FIG. 5. Left graph: comparison of $q(\Psi)$ for the two modes that coexist at $c = -0.645$. Right: contours of zero potential vorticity, which also mark the outermost closed streakline. The circles mark the mode with the nonlinear q–Ψ relationship in both panels; this mode has a smaller recirculation region than the other.

be an everywhere-analytic function. However, $F(\Psi)$ changes so smoothly from its open streakline behavior to its nonlinear form in the recirculation region that it is *possible* that $F(\Psi)$ is a C^∞ function, that is, one which is infinitely differentiable (though not analytic) at the outermost closed streakline (and everywhere else), and likewise B. However, it is possible that the potential vorticity and Bernoulli functions have discontinuities of the second or higher derivatives across the boundary of the recirculation region, which are simply not visible on the scatterplots.

Thus, the true mathematical character of $F(\Psi)$ and $G(\Psi)$ is still unknown. However, the combination of continuous slope and nonlinear, different-from-open-streakline behavior, has not been seen in geophysical vortices previously.

5. Comparison of coexisting $n = 1$ modes for $c = -0.645$

The mode illustrated above was computed by solving an initial value problem and marching until the flow had become approximately steady in a frame of reference moving with the vortex pair. Solitary waves were also computed by solving a nonlinear eigenvalue problem:

$$(u - c)u_x + vu_y - yv + h_x = 0 \tag{29}$$

$$(u - c)v_x + vv_y + yu + h_y = 0 \tag{30}$$

$$-ch_x + \{uh\}_x + \{vh\}_y = 0. \tag{31}$$

(We assume the solution is symmetric with respect to both x and y and impose the boundary conditions that $u, v \to 0$ and $h \to 1$ as $|x|, |y| \to \infty$.) Using the perturbative solution to initialize Newton's iteration, the nonlinear eigensolver converged to a *different* mode for the same value of c.

Figure 4 compares the streakfunctions for the two modes that coexist at this phase speed. Figure 5 shows the differences in the q–Ψ functional and in the size of the recirculation regions.

6. Westward-to-eastward instability runs

A westward-propagating *midlatitude* dipole on a midlatitude beta plane is subject to an instability that makes it curve around and eventually propagate eastward (Hesthaven et al. 1993). The reason is that when the line connecting the vortex centers is tilted at a slight angle relative to due north–south, the poleward movement strengthens the northern anticyclone and weakens the equatorward cyclone so that potential vorticity, $q \equiv (\zeta + f)/h$, is conserved as f decreases. The asymmetry forces the weakened cyclone to orbit clockwise around the stronger anticyclone, increasing the angle between the line connecting the vortex centers and a meridian. This creates a ''runaway'' that continues until the modon is moving eastward (or disintegrates). Araki et al. (1998) have done a linearized multipole analysis of the instability and argue that even eastward-traveling modons in midlatitude, which appear stable and robust in numerical experiments, are weakly unstable through a different mechanism.

Does this instability happen on the equatorial beta plane? Because dispersion and the equatorial waveguide are strong effects for near-equator vortices, it is by no means obvious that this instability will similarly wreck equatorially trapped vortex pairs.

Let $\tilde{u}(x, y)$ denote the usual analytical KdV soliton approximation to first order for $B = 0.8$. The initial condition used for this case was

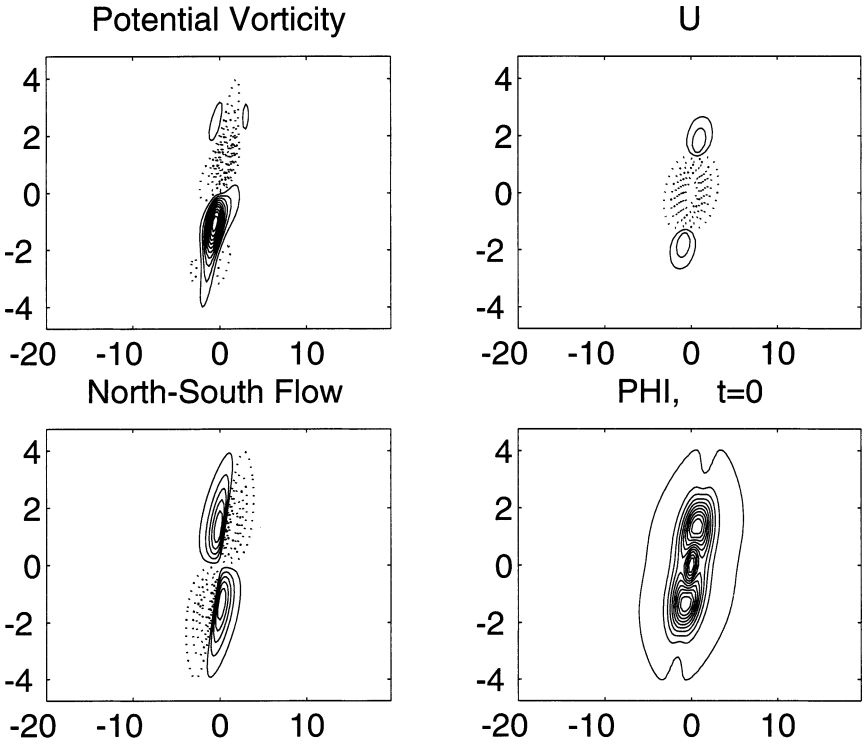

FIG. 6. Initial condition: tilted dipole. The potential vorticity illustrated is the anomaly, $q-\beta y$.

$$u(x, y) \equiv \tilde{u}(x - y/2, y). \tag{32}$$

This produced a somewhat asymmetric, ''tilted pair'' as illustrated in Fig. 6. An antisymmetric mode was rapidly radiated and then absorbed by the friction layers at the eastern and western boundaries of the model. There was a small but noticeable amount of rapidly spreading small-scale waves, probably gravity waves. At the time illustrated in Fig. 7, $t = 80$, the friction boundary layers [in the form of Eq. (21) with $\gamma_b = 1$, $\Xi = 1/4$] have absorbed most of the debris, and little except the modon is visible.

Although we have not completely explored the parameter space in the sense that one can imagine an infinite variety of finite amplitude perturbations, the case illustrated is typical of our experiments. Unlike its midlatitude brethren, the vortex pair is not unstable nor does it move latitudinally. Instead, the vortex pair rapidly symmetrizes itself by leaving the antisymmetric part behind as a wave packet.

7. Weakly nonlocal higher mode solitary waves

a. Background

Williams and Wilson (1988) tested the KdV/Rossby soliton theory of Boyd (1980a, 1985) through numerical solutions of the shallow-water wave equations. For the $n = 1$ latitudinal mode, there was good qualitative agreement, even at large amplitude. Solitary waves of different amplitudes collided elastically, just as predicted.

For higher mode solitary waves, there was a puzzle. For small amplitude, initialization of the flow with the lowest order perturbative approximation to the $n = 3$ solitary wave yielded a very robust and long-lived coherent structure. There was a stage of transient adjustment in which the quadrapole vortex shed a little radiation, and then the equilibrated soliton steadily translated without change in shape or amplitude for a very long time.

At moderate and large amplitude, however, the higher mode solitary waves decayed rapidly through radiation of sinusoidal Rossby waves of mode number $(n - 2)$. Boyd [(1989b); note that in (4.1b), 0.8266 should be 1.6532. The other results of this paper are not affected.] provided a theory: The *nonlinear* phase speed of the $n = 3$ solitary wave matches the *linear* phase speed of small amplitude sine waves in the $n = 1$ mode of zonal wavenumber $k \approx 2$. The resulting resonance forces the radiative decay of the solitary wave through emission of the resonant waves of lower latitudinal mode.

The amplitude of the emitted waves is an *exponential* function of the *reciprocal* of the soliton amplitude parameter ϵ. Thus, the $n = 3$ solitary wave is radiating for *all* amplitudes and there is *no stability threshold.* However, the rate of emission is so small for small ϵ as to be *invisible* in Williams and Wilson's numerical solution.

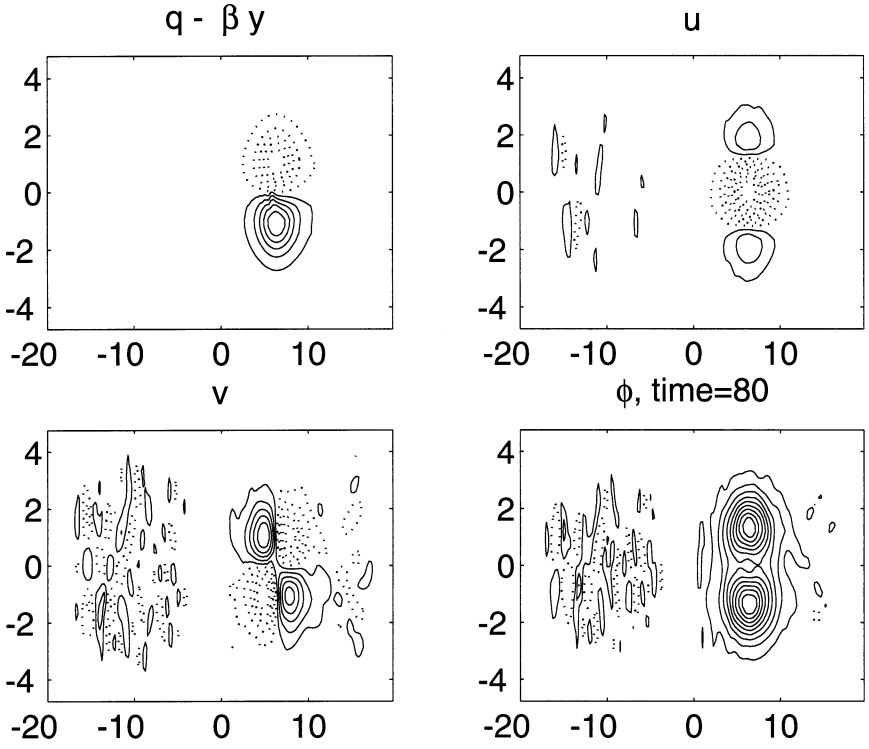

FIG. 7. Same as Fig. 6 (initially tilted equatorial dipole) but showing the flow at $t = 80$. An antisymmetric mode was quickly radiated; it disappeared by the time shown here because it was absorbed by the damping boundary layers. The potential vorticity in the upper left panel is the PV anomaly; i.e., it is the total potential vorticity minus the ambient vorticity: βy for $x \in [0, 40]$, $y \in [-5, 5]$, 160×41 grid, time step = 1/100. The model used a frame of reference traveling at $c_{\text{trans}} = -0.55$ so as to keep the dipole roughly centered in the computational domain. A sixth-order hyperviscosity, which creates an *e*-folding decay timescale of 1/2 for the two grid-scale waves, was used; this had a negligible effect on larger features, which is why the plot shows some debris. A strong friction at the east-west boundaries was used to create "sponge layers" to absorb some of the radiative transients as described in the text.

The leakage includes Rossby waves of all lower odd n, but the amplitude of modes lower than $(n - 2)$ is exponentially small compared to emission in the $(n - 2)$ mode, so only a single mode of radiation was detectable.

Williams (1996) has shown through numerical solutions of a baroclinic model that solitary waves in the $n = 1$ latitudinal mode and the first baroclinic mode are weakly nonlocal through radiative leakage into the barotropic mode. (In theory, higher latitudinal modes should decay similarly.) However, there has never been a careful numerical confirmation of the radiative decay of higher latitudinal modes in the shallow water equations.

b. Initial value experiments

We therefore ran our model with an initial condition equal to the $n = 3$ zeroth-order solitary wave (Boyd 1980a) for $\epsilon = 1/3$ [$B = 1/3$ in the notation of the earlier article]. Results are shown in a frame of reference which moves at the predicted phase speed of the solitary wave, $c_{\text{sol}} = -1/7 - 0.08\epsilon^2$, so that the core of the coherent structure remains centered at $x = 0$.

Figure 8 shows that the expected wavepacket does indeed emerge. The amplitude of the radiation is very small, however, and only that for the north–south current is readily visible. The radiation is noticeably more confined in latitude than the core of the solitary wave, which has the structure of the second lowest symmetric mode. It follows that the radiation lies almost entirely in the $n = 1$ mode as predicted.

The resonance condition is

$$c_{\text{sol}} = \frac{-1}{k^2 + 3}, \tag{33}$$

where the right-hand side is the (approximate but very accurate) dispersion relation for infinitesimal amplitude $n = 1$ Rossby waves of zonal wavenumber k. This predicts the wavelength of the emission to be

$$k_{\text{res}} = 2\frac{\sqrt{1 + 0.14\epsilon^2 - 0.235\epsilon^4}}{1 + 0.56\epsilon^2}, \tag{34}$$

which is $k_{\text{res}} \approx 1.895$ for $\epsilon = 1/3$.

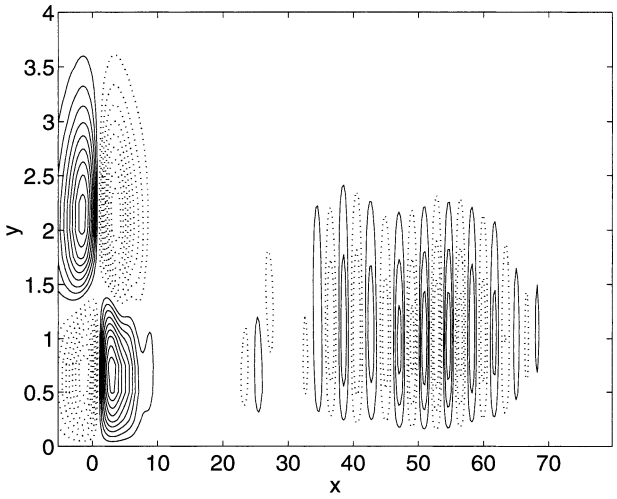

FIG. 8. Isolines of the north–south velocity at $t = 400$. Negative-valued contours are dashed. Computations were performed in a frame of reference moving at the perturbatively predicted phase speed of the solitary wave, so the quadrapole pattern which is the core of the soliton remains centered at $x = 0$. The computational interval extended from $x \in [-80, 80]$, but only part of this domain is illustrated.

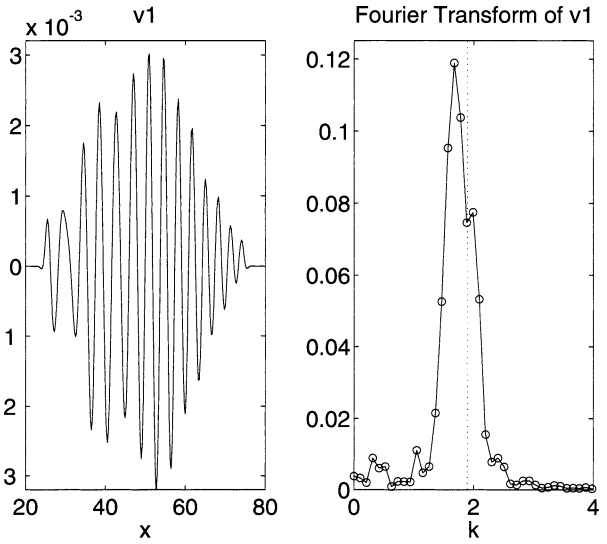

FIG. 9. Left: the coefficient $v_1(x)$ of the first degree Hermite function of the north–south current after multiplication by the ''window'' function $W = (1/2)\,[\mathrm{erf}(x - 25) - \mathrm{erf}(x - 75)]$. Right: Fourier transform of the windowed wavepacket. The vertical dotted line denotes the predicted resonant wavenumber $k \approx 1.895$.

By multiplying the wavepacket by a windowing function, it is possible to take the Fourier transform of the packet with minimal contamination from the core of the solitary wave. When the north–south current is expanded in Hermite functions, the jth coefficient is the sum of three latitudinal modes. However, because our initial condition is a nonlinear Rossby wave, the gravity wave modes are only weakly excited. It thus a good approximation to take the amplitude of the $n = 1$ Hermite coefficient of v as the amplitude of the $n = 1$ Rossby mode. Figure 9 shows the Fourier transform of the windowed wavepacket indeed has a peak close to the predicted $k = 1.895$.

The group velocity in an earth-fixed frame of reference is $c_g = (3 - k^2)/(3 + k^2)^2$. Relative to the core of the solitary wave, and therefore in the moving reference frame,

$$c_g^{\text{relative}} \approx \frac{1}{7} + 0.08\epsilon^2 + \frac{k_{\text{res}}^2 - 3}{(k_{\text{res}}^2 + 3)^2}, \qquad (35)$$

which is approximately 1/6. Thus, over the length of the integration, which is 400 nondimensional time units, the emitted radiation should spread eastward relative to the solitary wave about 66 spatial units, which is only a slight underestimate.

The one puzzle is that the envelope of the wave packet does not show a constant amplitude, as expected, but instead diminishes to almost nothing close to the solitary wave. Similar fluctuations have been seen in other weakly nonlocal solitary waves such as the ϕ^4 breather (Boyd 1998b), but the cause is not understood.

c. Nonlinear eigenvalue solutions

It is also possible to solve for the $n = 3$ mode as the steadily translating solution to a nonlinear eigenvalue problem. In an ocean basin, this is rather artificial: such steadily propagating coherent structures are east–west symmetric with respect to the center of the core, and thus have small amplitude $n = 1$ waves *west* of the core. This is possible only in a landfree ocean where the eastward radiating $n = 1$ waves are free to expand around the globe until they reach the core from the west.

In spite of its artificiality, such nonlinear eigensolutions (with periodic boundary conditions in the east–west) have been very useful in the general theory of nonlocal coherent structures as reviewed in the monograph (Boyd 1998b). The outside-the-core oscillations of the nonlocal solitary waves confirm that the radiation is an intrinsic part of the dynamics, and not merely a transient feature that might disappear from an initial value calculation if only it were run longer.

Figure 10 shows the result of such a computation. [The numerical intricacies are described in Boyd (2002; 1998b).] The rather eccentric value of the phase speed was the result of intializing the iteration with the perturbative solution of Boyd (1980a) for $n = 3$ mode with $B = 3/8$, that is, the east–west structure proportional to $\mathrm{sech}^2[0.375(x - ct)]$. Other calculations, not shown, demonstrate that the amplitude of the $n = 1$ oscillations falls exponentially fast with decreasing amplitude in the core of the structure. For larger core amplitude (or a more negative c), the far field oscillations are as big or bigger than the core, at least in the north–south flow, and the solitary wave is no longer ''weakly'' nonlocal.

For this moderate amplitude, however, we have con-

firmation that this latitudinal mode indeed has weakly nonlocal solitary waves. The eigensolutions are fully consistent with the initial value experiments of Williams and Wilson (1988) and our own initial value experiments here.

The general theory of weakly nonlocal waves has many subtleties, such as those associated with the quantization effects of periodic boundary conditions, which we cannot discuss here. These issues are fully explained in the monograph (Boyd 1998b) and the review articles (Boyd 1989a, 1991b, 1999).

8. A guide for soliton hunters

Identifying solitary waves in the ocean is difficult for several reasons:

1) Solitons often form in closely spaced clusters; the adjective ''solitary'' is a misnomer.
2) The timescale for formation of a weak soliton may be larger than the transpacific transit time.
3) It may be difficult, on a finite timescale, to distinguish solitary waves from dispersing, transient waves.
4) The structure and phase speed of Rossby solitary waves will be significantly modified by the strong equatorial mean currents.
5) Solitons may already have been discovered, but identified as something else.

a. The unsolitary soliton

A Rossby solitary wave decays exponentially fast both eastward and westward from its peak. Consequently, two solitons may be very close, and yet have very little dynamical interaction.

The concept of a train of closely packed solitary waves seems a semantic contradiction. A ''solitary'' wave conveys the mental image of a single tall peak, ''alone on a wide, wide sea,'' to quote Coleridge's *Rhyme of the Ancient Mariner.*

However, the Korteweg–de Vries equation also has solutions that are *periodic* in longitude, the so-called ''cnoidal waves.'' These are a one-parameter family of shapes described by elliptic functions. In the limit that the elliptic modulus $m \to 0$, the cnoidal wave is a sinusoidal wave of infinitesimal amplitude. In the limit, for fixed spatial period, that m tends to its maximum value of one, the peaks of the cnoidal wave become infinitely tall and thin, and each peak is equal both in shape and speed to the solitary wave.

The subtlety is that the sinelike and soliton-like regimes *strongly overlap.* The overlap is strongest for $m = 1/2$ (Boyd 1982). For this special case, the elliptic functions are squares of the cosine-lemniscate function named by Gauss in 1797. The approximation of the ''lemniscoidal wave'' phase speed c_{lemnisc} by the speed of an infinitesimal amplitude sine wave is accurate to within 5%, so this KdV solution is only a slight perturbation of a sine wave. However, the spatial structure of all cnoidal waves, including the lemniscoidal wave as a special case, is *exactly* given by the superposition of an infinite number of evenly spaced solitary waves (Toda 1975). The phase speed of the cnoidal wave is altered by the mutual interaction of the solitons, but for the lemniscoidal case, the soliton–soliton interaction is so weak that c_{lemnisc} is approximated by the speed of one of its constituent solitary waves to 5% also. Thus, the lemniscoidal wave is *both soliton and sine wave* to within an error of no worse than 1 part in 20 for its phase speed.

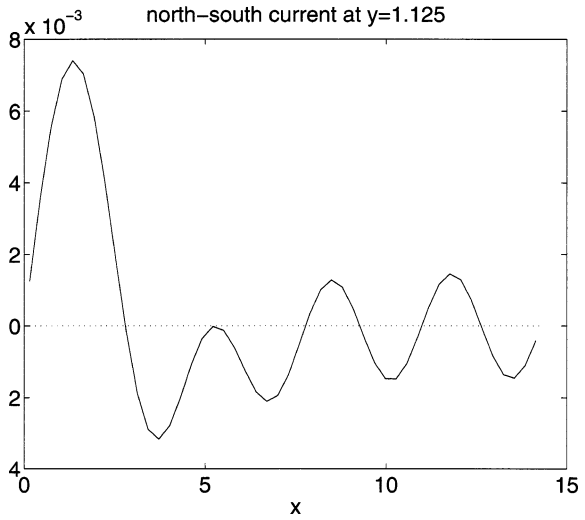

FIG. 10. Nonlinear eigenvalue solution for $c = -0.15411$: the north–south current at a particular latitude, $y = 1.125$, is plotted vs longitude. The calculation used a 48×24 grid with centered eighth-order differences on the domain $x \in [0, 4.25W_f] \otimes y \in [0, 6]$, where $W_f = 2\pi/k_{\text{res}}$ is the predicted wavelength of the far field oscillations in the $n = 1$ latitudinal Rossby mode. Both u and ϕ were assumed symmetric with respect to both the x and y axes; v was doubly antisymmetric.

The label ''solitary wave'' is a terminological atrocity. A flow with many closely spaced peaks may be the superposition of solitons that have only a weak mutual interaction in spite of close proximity. Unfortunately, this implies that a search for isolated peaks, ''alone on a wide, wide sea,'' is far too narrow.

b. Formation and dispersing transients

The Korteweg–de Vries equation can be exactly solved for a general initial condition using the so-called ''inverse scattering'' method. This asserts that an arbitrary initial condition will *always* generate *at least one soliton* unless the initial condition is special or nongeneric in some sense. The only important class of nonsoliton-generating initial conditions are those that are *everywhere nonpositive,* which in the present context is a perturbation of the main thermocline that everywhere thins the upper mixed layer. If a perturbation both deep-

ens and thins the mixed layer, or only deepens the upper layer, then at least one solitary wave will *asymptotically* evolve.

There are two complications. The general solution to the KdV equation consists of one or more solitary waves plus a wave train that eventually disperses to nothing. As $t \to \infty$, each solitary wave, traveling at a unique phase speed, will separate itself more and more from other solitary waves and from the dispersing transients, which travel more slowly than any soliton. [In our context, the tallest (and therefore fastest) solitary wave is the western edge of the waves that evolve from a spatially localized initial condition; moving westward at group velocities in range of infinitesimal amplitude waves, the dispersing transients will be eastward of all the solitary waves.] The first complication is that the time for this ''separation-by-speed'' is inversely proportional to the amplitude of the disturbance. Thus, a weak, broad pulse may not evolve into clearly distinguishable solitary waves until a time far longer than the transpacific crossing time.

There are a couple of consolations. First, if the initial disturbance is sufficiently large, the solitary wave, or at least the tallest soliton, will evolve so quickly that an animation of the flow will suffice to identify it as a soliton, separating westward from the roil of smaller solitons and dispersing transients to its east. If, on the other hand, the disturbance is small and slowly evolving, the Korteweg–de Vries perturbation theory of Boyd (1980a) should be an accurate approximation. One can then identify the number of solitary waves by solving a one-dimensional linear eigenvalue problem, that is, the stationary Schroedinger equation with the longitudinally varying amplitude of the $n = 1$ Rossby wave as the negative of the potential energy, as explained in our earlier article. It is quite unnecessary in the KdV regime to resort to time-dependent solutions of the full shallow-water wave equations.

The second consolation is that there is an even easier way to determine when nonlinear effects are important as explained in the next subsection.

c. Breaking/nonbreaking spoor of nonlinear flow

If Rossby waves were not dispersive, then nonlinearity would cause these waves to steepen and break. It is much easier to predict breaking for a nondispersive system than it is to predict the evolution of waves under the joint influence of both dispersion and nonlinearity. The KdV theory of Boyd (1980a), combined with the known theory of the one-dimensional advection equation reviewed in Boyd (1980b), shows that the *dispersion-ignored* criterion for the $n = 1$ Rossby mode to break is

$$t_B = \frac{1.46}{\max\{u_x\}}, \tag{36}$$

where the maximum of the slope of the zonal velocity is evaluated at $t = 0$. If we define an initial zonal length scale L such that the maximum slope of u is $\max(u)/L$, then the breaking condition becomes

$$t_B = \frac{1.46L}{\max(u)}. \tag{37}$$

The breaking formula is of course a fantasy because Rossby waves *are* dispersive. Still, if the formula predicts that a disturbance should break, and it does not, then *dispersion must be as important as nonlinearity*, and this is a characteristic of solitary waves.

The nondimensional width of the Pacific Ocean is about 35, and the nondimensional phase speed of a (linear) Rossby long wave is $O(-1/3)$. Thus, a disturbance of $O(1)$ width would break, were it not for dispersion, even if the initial nondimensional zonal velocity of the pulse is rather small. We shall give a concrete illustration of the breaking formula in the next subsection.

d. Misidentification

Since ocean peaks do not wave little signs labeled ''I'm a solitary wave! I'm a solitary wave!,'' it is always possible that equatorial solitons have already been observed but not identified as such. The equatorial plumes on Jupiter, for example, had been observed many years before Showman and Dowling (2000) showed through numerical modeling that nonlinearity was essential in explaining the observed longevity of the plumes; infinitesimal amplitude Rossby waves of the same wavelength would disperse much faster than observed.

The most prominent coherent structures in the tropical ocean are known variously as ''Legeckis eddies'' or ''tropical instability waves.'' Discovered first in satellite sea surface temperature measurements in the late 1970s, the most thorough observational study to date is Kennan and Flament (2000). These eddies form through shear instability between the South Equatorial Current (SEC) and the North Equatorial Countercurrent (NECC) and evolve to approximately axisymmetric anticyclonic vortices centered about 4.5° (1.5 nondimensional units) off the equator with a typical diameter of about 500 km (1.6 nondimensional) with maximum tangential velocities of about 60 cm s^{-1} (about 0.3 nondimensional).

The $n = 1$ latitudinal mode Rossby solitary wave also consists of a near-equator anticyclonic vortex in the Northern Hemisphere (plus a contrarotating vortex in the Southern Hemisphere). Although the ''time-of-breaking'' formula neglects the strong mean currents, it still is interesting, at least for purposes of order-of-magnitude estimate, to apply it to Legeckis eddies. Taking the radius of the eddy as the length scale L, one finds

$$t_B \approx 4. \tag{38}$$

This is smaller than the transpacific crossing time by a factor of roughly 25! Clearly, Legeckis eddies are strongly nonlinear, a fact that is hardly a surprise to the observationalists. However, we can say more: the ap-

parent absence of steep fronts on the western edge of the eddies implies that dispersion must also be important for these waves.

We conjecture that mature tropical instability waves are solitary waves.

9. Open problems

The most important unresolved problem is: Why are equatorial Rossby waves so readily observed in numerical models and theory, but not in the ocean? The intense vertical and latitudinal shear and vertical stratification of the ocean are obvious candidates as possible ''soliton suppressors.'' However, Marshall and Boyd (1987), following work by others on solitons in continuous stratification in other contexts, showed that vertical density variations are only a slight complication. [The solitons become weakly nonlocal through radiation in the barotropic mode as illustrated in Fig. 1 of Williams (1996) and discussed in Boyd (1998b).] Similarly, shear will alter modal structure (Greatbatch 1985; M.-T. Li 1983, unpublished manuscript; Li 1984) but not restrict or suppress solitary waves even with critical latitudes (Redekopp 1977).

We have shown here that solitons exist even at very large amplitudes. Furthermore, the tilt instability, known to be strong for westward-propagating midlatitude modons, has been shown here to be suppressed by the equatorial waveguide.

Perhaps, as noted in the previous section, the anticyclonic vortices known variously as Legeckis eddies or tropical instability waves are, in fact, solitary waves, at least in their mature stage.

To confirm or disprove this conjecture, and to find other possible soliton-suppressing mechanisms, it will be necessary to repeat this study with mean shear currents. This is difficult because the equatorial currents vary strongly with depth as well as latitude, so it would be highly desirable to use a three-dimensional model, as opposed to the two-dimensional shallow-water system solved here. Furthermore, both nonlinear effects and dispersion will be sensitive to the currents, so it will be necessary to explore a range of currents, and hope that the qualitative conclusions are the same for all reasonable mean currents.

For now, the mystery of the missing equatorial solitons remains unsolved.

Acknowledgments. This work was supported by NSF Grants OCE9521133 and OCE9986368. I thank the reviewers for helpful comments.

REFERENCES

Araki, K., S. Toh, and T. Kawahare, 1998: Stability of a modon structure: Multipole expansion analysis. *Wave Motion,* **28,** 69–78.

Batchelor, G. K., 1956: On steady laminar flow with closed streamlines at large Reynolds number. *J. Fluid Mech.,* **1,** 177–190.

Boyd, J. P., 1980a: Equatorial solitary waves. Part I: Rossby solitons. *J. Phys. Oceanogr.,* **10,** 1699–1718.

——, 1980b: The nonlinear equatorial Kelvin wave. *J. Phys. Oceanogr.,* **10,** 1–11.

——, 1982: Theta functions, Gaussian series, and spatially periodic solutions of the Korteweg-de Vries equation. *J. Math. Phys.,* **23,** 375–387.

——, 1983a: Equatorial solitary waves. Part II: Envelope solitons. *J. Phys. Oceanogr.,* **13,** 428–449.

——, 1983b: Long wave/short wave resonance in equatorial waves. *J. Phys. Oceanogr.,* **13,** 450–458.

——, 1983c: Second harmonic resonance for equatorial waves. *J. Phys. Oceanogr.,* **13,** 459–466.

——, 1984: Equatorial solitary waves. Part IV: Kelvin solitons in a shear flow. *Dyn. Atmos. Oceans,* **8,** 173–184.

——, 1985: Equatorial solitary waves. Part 3: Westward-traveling modons. *J. Phys. Oceanogr.,* **15,** 46–54.

——, 1989a: New directions in solitons and nonlinear periodic waves: Polycnoidal waves, imbricated solitons, weakly non-local solitary waves and numerical boundary value algorithms. *Advances in Applied Mechanics,* T. Y. Wu and J. W. Hutchinson, Eds., Vol. 27, Academic Press, 1–82.

——, 1989b: Non-local equatorial solitary waves. *Mesoscale/Synoptic Coherent Structures in Geophysical Turbulence: Proceedings of the 20th Liege Colloquium on Hydrodynamics,* J. C. J. Nihoul and B. M. Jamart, Eds., Elsevier, 103–112.

——, 1991a: Nonlinear equatorial waves. *Nonlinear Topics of Ocean Physics: Fermi Summer School, Course LIX,* A. R. Osborne, Ed., North-Holland, 51–97.

——, 1991b: Weakly non-local solitary waves. *Nonlinear Topics of Ocean Physics: Fermi Summer School, Course LIX,* A. R. Osborne, Ed., North-Holland, 527–556.

——, 1998a: High order models for the nonlinear shallow water wave equations on the equatorial beta-plane with application to Kelvin wave frontogenesis. *Dyn. Atmos. Oceans,* **28** (2), 69–91.

——, 1998b: *Weakly Nonlocal Solitary Waves and Beyond-All-Orders Asymptotics: Generalized Solitons and Hyperasymptotic Perturbation Theory.* Mathematics and Its Applications, Vol. 442, Kluwer, 608 pp.

——, 1999: The devil's invention: Asymptotics, superasymptotics, and hyperasymptotics. *Acta Applicandae,* **56,** 1–98.

——, 2002a: Generalized Newton iterations for formally-overdetermined determinate discretizations of nonlinear eigenproblems for solitary and cnoidal waves. *J. Comput. Phys.,* in press.

——, 2002b: Weakly nonlocal equatorial Kelvin fronts and solitons. *J. Phys. Oceanogr.,* submitted.

Domaracki, A., and A. Loesch, 1977: Dynamics of closed systems of resonantly interacting equatorial waves. *J. Atmos. Sci.,* **34,** 486–498.

Fedorov, A. V., and W. K. Melville, 2000: Kelvin fronts on the equatorial thermocline. *J. Phys. Oceanogr.,* **30,** 1692–1705.

Greatbatch, R. J., 1985: Kelvin wave fronts, Rossby solitary waves and nonlinear spinup of the equatorial oceans. *J. Geophys. Res.,* **90,** 9097–9107.

Haidvogel, D. B., and A. Beckmann, 1999: *Numerical Ocean Circulation Modeling.* Environmental Science and Management, Vol. 2, Imperial College Press, 320 pp.

Hesthaven, J. S., J. P. Lynov, and J. Nycander, 1993: Dynamics of nonstationary dipole vortices. *Phys. Fluids,* **5A,** 622–629.

Jain, R. K., B. N. Goswami, V. Satyan, and R. N. Keshavamurty, 1981: Envelope soliton solution for finite-amplitude equatorial waves. *Proc. Indian Acad. Sci., Earth Planet. Sci.,* **90,** 305–326.

Kennan, S. C., and P. J. Flament, 2000: Observations of a tropical instability vortex. *J. Phys. Oceanogr.,* **30,** 2277–2301.

Kindle, J., 1983: On the generation of Rossby solitons during El Nino. *Hydrodynamics of the Equatorial Ocean,* J. C. J. Nihoul, Ed., Elsevier, 353–368.

Li, M.-T., 1984: Equatorial solitary atmospheric waves in meridional shear flow. *Tropical Ocean–Atmos. Newsl.,* **1** (23), 15–16.

Loesch, A., and R. C. Deininger, 1979: Dynamics of closed systems

of resonantly interacting equatorial waves. *J. Atmos. Sci.,* **36,** 1490–1497.
Long, B., and P. Chang, 1990: Propagation of an equatorial Kelvin wave in a varying thermocline. *J. Phys. Oceanogr.,* **20,** 1826–1841.
Ma, H., 1992: The equatorial basin response to a Rossby wave packet: The effects of nonlinear mechanism. *J. Mar. Res.,* **50,** 567–609.
——, 1996: The dynamics of North Brazil Current retroflection eddies. *J. Mar. Res.,* **54,** 35–53.
Mallier, R., 1994: Stuart vortices in a stratified mixing layer. 1. The Garcia model. *Geophys. Astrophys. Fluid Dyn.,* **74,** 73–97.
——, 1995: Stuart vortices on a beta-plane. *Dyn. Atmos. Oceans,* **22** (4), 213–238.
Marshall, H. G., and J. P. Boyd, 1987: Solitons in a continuously stratified equatorial ocean. *J. Phys. Oceanogr.,* **17,** 1016–1031.
Matsuura, T., and T. Yamagata, 1985: A numerical study of a viscous flow past a circular cylinder on an f-plane. *J. Meteor. Soc. Japan,* **63,** 151–167.
——, and S. Iizuka, 2000: Zonal migration of the Pacific warm-pool tongue during El Niño events. *J. Phys. Oceanogr.,* **30,** 1582–1600.
Milewski, P. A., and E. G. Tabak, 1999: A reduced model for nonlinear dispersive waves in a rotating environment. *Geophys. Astrophys. Fluid Dyn.,* **90,** 139–159.
Moore, D. W., and P. P. Niler, 1974: A two layer model for the separation of inertial boundary currents. *J. Mar. Res.,* **32,** 457–484.
——, and S. G. H. Philander, 1977: Modelling of the tropical oceanic circulation. *The Sea,* E. D. Goldberg, Ed., *Marine Modelling,* Vol. 6, Wiley and Sons, 319–361.
Redekopp, L. G., 1977: On the theory of solitary Rossby waves. *J. Fluid Mech.,* **82,** 725–745.
Ripa, P., 1982: Nonlinear wave–wave interactions in a one-layer reduced-gravity model on the equatorial beta-plane. *J. Phys. Oceanogr.,* **12,** 97–111.
——, 1983a: Resonant triads of equatorial waves in a one-layer model. Part I: Non-local triads and triads of waves with the same speed. *J. Phys. Oceanogr.,* **13,** 1208–1226.
——, 1983b: Resonant triads of equatorial waves in a one-layer model. Part II: General classification of resonant triads and double triads. *J. Phys. Oceanogr.,* **13,** 1227–1240.
——, 1985: Nonlinear effects in the propagation of Kelvin pulses across the Pacific Ocean. *Advances in Nonlinear Waves,* L. Debnath, Ed., Pitman, 43–56.
Showman, A. P., and T. E. Dowling, 2000: Nonlinear simulations of Jupiter's 5-μm hot spots. *Science,* **289,** 1737–1740.
Toda, M., 1975: Studies of a nonlinear lattice. *Phys. Rep.,* **18,** 1–124.
Williams, G. P., 1996: Jovian dynamics. Part I: Vortex stability, structure, and genesis. *J. Atmos. Sci.,* **53,** 2685–2734.
——, and R. J. Wilson, 1988: The stability and genesis of Rossby vortices. *J. Atmos. Sci.,* **45,** 207–249.
Wu, R., 1986: Long wave approximation, linear and non-linear Rossby waves. *Sci. Sin.,* **29** (3), 302–312.
Yamagata, T., 1981: Generalization of Prandtl-Batchelor theorem for planetary fluid flows in a closed geostrophic contour. *J. Meteor. Soc. Japan,* **59,** 615–619.
Zheng, Q., R. D. Susanto, X. H. Yan, W. T. Liu, and C. R. Ho, 1998: Observation of equatorial Kelvin solitary waves in a slowly varying thermocline. *Nonlinear Processes Geophys.,* **5** (3), 153–165.